# Near-infrared inorganic/organic optical upconverter with an external power efficiency of>100%

Chen, Jun; Ban, Dayan; Helander, Michael G.; Lu, Zheng-Hong; Poole, Philip



**Publisher's version / Version de l'éditeur:**
https://doi.org/10.1002/adma.201001946
*Advanced materials, 22, 43, pp. 4900-4904, 2010-11-16*

# Near-Infrared Inorganic/Organic Optical Upconverter with an External Power Efficiency of >100%

By *Jun Chen, Dayan Ban,* Michael G. Helander, Zheng-Hong Lu,* and *Philip Poole*

Imaging devices in the near-infrared (NIR) have become increasingly important in many applications, such as night vision, range finding, and semiconductor wafer inspection.[1–3] The spectral region around 1.5 μm is of particular commercial interest due to the low water absorption in this range. Currently, the industry standard is to use an InGaAs photodetector (PD) interconnected with a silicon read out integrated circuit using indium bump technology.[4] An alternative method is based on a NIR optical upconverter, which converts NIR radiation to a shorter wavelength (e.g., 1 μm or below) that can be effectively detected by a conventional silicon (cutoff wavelength about 1 μm) charge coupled devices (CCD).[5] Such an optical upconverter combined with a commercially available CCD functions as an ordinary infrared camera. Liu *et al.* fabricated the inorganic NIR-to-visible upconverter by integrating a GaAs light-emitting diode (LED) and InGaAs/InP PD.[1] However, in monolithic devices created by direct epitaxial growth, the bandgap difference between the active region of the LED and the active region of the photodetector is highly restricted due to the stringent lattice-matching requirements imposed by the uninterrupted epitaxial growth of the various layers in the devices. This resulted in low efficiency and limited range of upconversion from 1.5 μm to 1.0 μm. In contrast, organic semiconductors have advantages over epitaxial structures for the fabrication of large-area devices because of their simplified process handling. As each organic molecule is a topologically perfect structure, the growth of each organic layer does not require "lattice matching". Kim *et al.* demonstrated an all organic infrared upconversion device using a tin phthalocyanine (SnPc):$C_{60}$ bulk heterostructure layer as NIR PD and a fac-tris(2-phenylpyridinato)iridium (III) ($Irppy_3$)-doped 4,4-N,N-dicarbazole-biphenyl (CBP) green-phosphorescent organic light-emitting diode (OLED).[6] However, neither small molecules nor polymers with low bandgaps are currently available for the manufacture of efficient photodiodes in the spectral region above 1 μm,[7] and the maximum reported upconversion efficiency of the organic NIR upconversion device was only 2.7% under 830 nm infrared light.[6] Targeting to make low-cost, large-area upconversion device which operates in the 1.5 μm region (e.g. covering 1.2–1.6 μm), we proposed an organic/inorganic hybrid upconversion device that was made by direct tandem integration of an inorganic InGaAs/InP PD with an OLED.[8,9] The hybrid device converted infrared light in the eye-safe region at 1.5 μm in wavelength to visible light, which is observable to naked human eyes. Moreover, this integrated device combined the flexibility of organic semiconductors and the high NIR photoresponsivity of InGaAs/InP inorganic semiconductor heterostructures. The overall upconversion efficiency was still limited by the low extraction efficiency in the OLED. In order for the upconversion scheme to be more attractive, high efficiency optical upconverter is surely desired.

In this paper, we report a new upconverter structure with a built-in gain mechanism, a hybrid optical upconverter that integrates a *p-n-p* InGaAs/InP heterojunction phototransistor (HPT) and an OLED. Incoming 1.5 μm light is absorbed by the HPT component. The generated photocarriers are amplified in the HPT and then injected into the OLED to emit visible light (green), depending on different organic emissive materials used (**Figure 1a**). In this hybrid device, the *p*-doped collector of the HPT functions as the anode of the OLED. As there is no intrinsic charge carrier in the organic molecules, all charge carriers have to be injected from the cathode and the anode (Figure 1b). The injection of holes from the collector is modulated by incoming 1.5 μm light. The layer structures and doping profiles of the HPT component were carefully designed to improve the electrical gain. With the incorporation of sufficient internal gain, the intensity of output visible light was greater than that of the input NIR light. To our best knowledge, this is the first compact device that functions not only as a NIR wavelength upconverter, but also as an optical power amplifier.

An HPT is basically a heterojunction bipolar transistor with a light sensitive collector and base region. Figure 1c shows the schematic diagram of a *p-n-p* InGaAs/InP HPT structure that we will refer to in this paper (Forward-bias emitter-base junction and reverse-bias collector-base junction). 1.5 μm light is absorbed in the narrow bandgap collector and base region,

[*] J. Chen, Prof. D. Ban
Department of Electrical and Computer Engineering
University of Waterloo
200 University Avenue West
Waterloo, N2L 3G1 (Canada)
E-mail: dban@uwaterloo.ca.
M. G. Helander, Prof. Z.-H Lu
Department of Materials Science and Engineering
University of Toronto
184 College Street
Toronto, M5S 3E4 (Canada)
Prof. Z.-H Lu
Department of Physics
Yunnan University
2 Cuihu Beilu, Yunnan
Kunming 650091 (P. R. China)
Dr. P. Poole
Institute for Microstructural Sciences
National Research Council
1200 Montreal Road
Ottawa, K1A 0R6 (Canada)

DOI: 10.1002/adma.201001946

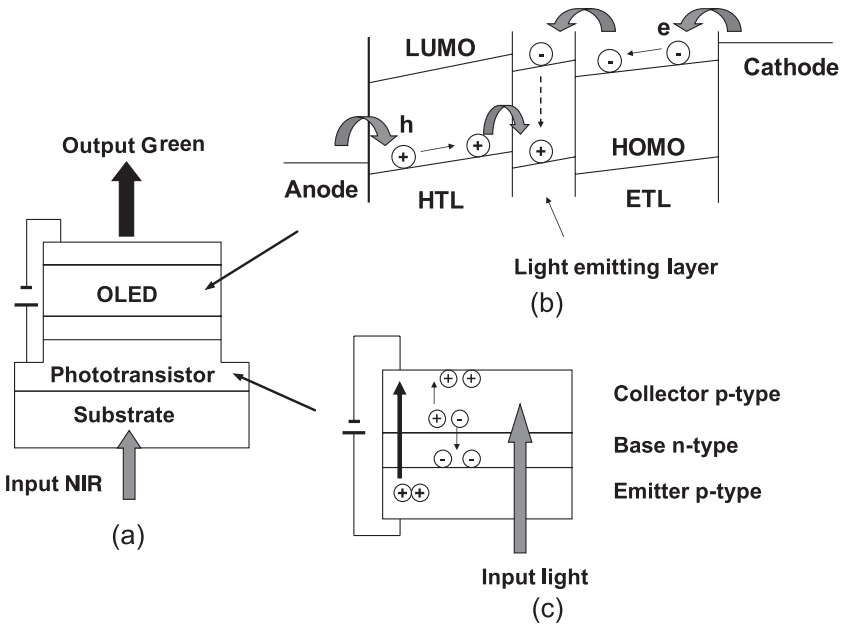


**Figure 1.** (a) Schematic diagram of a hybrid upconversion device; (b) Energy diagram of an OLED; (c) Schematic diagram of a *p-n-p* HPT structure (forward-bias emitter-base junction and reverse-bias collector-base junction).

producing electron-hole pairs. Subsequently, holes drift toward the collector while electrons drift toward the floating-base region due to a built-in junction field. Electrons accumulate in the base and these extra charges forward bias the base-emitter junction, causing more holes to be injected from the *p*-InP emitter. Some of the injected holes are lost in the base due to the recombination with electrons but most of the injected holes diffuse across the thin base layer and reach the base-collector depletion region, leading to an optical gain. The overall optical gain can be expressed as follows,

$$g = \frac{I_C}{q}\frac{h\nu}{P_{in}} = \eta(1+\beta) \quad (1)$$

here $h\nu$ is the photon energy at the incident light wavelength, $P_{in}$ incident light power, $I_C$ collector current, $\eta$ the quantum efficiency, and $\beta$ the common emitter current gain, which is governed by emitter injection efficiency and base transport factor,

$$\beta = \frac{\eta_e}{1-\eta_e} = \frac{I_p}{I_r} \quad (2)$$

where $\eta_e$ is emitter injection efficiency, and $\beta$ is equal to the ratio of total current injected from the emitter to the base ($I_p$) and the recombination current ($I_r$) in the emitter-base heterojunction. For a higher optical gain, the emitter injection efficiency must be enhanced by minimizing the recombination current. When $\eta_e \approx 1.0$, $\beta$ is theoretically given by $\beta = 1/[\cosh(W_B/L_p)\text{-}1]$. $W_B$ is the base width and $L_p$ is the hole diffusion length in the base layer.[10,11] In that case, the current gain is determined by the base width ($W_B$). The thinner the base layer, the higher the current gain $\beta$. The device structure optimization point of this work is achieved by the following: (i) reduction of the base layer thickness, and (ii) increase of hole injection efficiency from the emitter.[12] We adopted double emitter layers (high-low doping profiles) to suppress recombination current at the interface of the emitter/base, so that the hole injection efficiency could be improved.[13] (see Supporting information, Figure S1.)

The optimized HPT was grown and integrated with an OLED to form a hybrid upconversion device (**Figure 2a**). A metal mirror (Ti/Au) was embedded between the HPT and the OLED to form a good contact and also to enhance input light absorption efficiency as well as output light emission efficiency.[9] As shown in Figure 2b, the spontaneous emission from the OLED is random in radiative direction. With a high-reflectivity metal layer underneath the OLED, the photons that are originally emitted downward will be bounced back at the OLED/metal interface. After changing directions, this portion of the photons can contribute to the top emission of the device thus enhancing the OLED efficiency. The absorption efficiency of the HPT side could also be enhanced in a similar way with the insertion of such a metal layer. **Figure 3** shows the luminance-voltage (*L-V*) curve of this upconversion device under 1.5 μm infrared illumination with a power density of 1.2 mW/cm$^2$. Incoming 1.5 μm optical radiation was absorbed by the HPT, generating an amplified photocurrent. The resultant photocurrent drove the OLED that emits green light. The integrated device started to turn on at a low bias (~6 V). This shows that efficient hole injection from the semiconductor to the organic layers was achieved via the floating metal contact (also the embedded mirror). The inset of Figure 3 is an image of the hybrid upconverter operating at 15 V with input NIR from bottom. As the device bias continued to increase, the output luminance of the green emission (peaked at ~564 nm) increased rapidly up to 9000 cd/m$^2$. The rapid increase of the luminance was mainly due to the increase of the photocarrier collection efficiency and internal electrical gain, which was enhanced by the additional external voltage that dropped across the HPT component.

**Figure 4a** shows the measured photocurrent density (total current density minus dark current density) as a function of device bias under 1.5 μm infrared radiation (1.2 mW/cm$^2$), together with the calculated responsivity of the HPT component. The responsivity started to rise at 6 V and gradually increased with further increase of the device bias. At 21 V bias (the total voltage dropped across the HPT component and the OLED component), the responsivity was measured to be 47 A/W under input infrared radiation of 1.2 mW/cm$^2$. In comparison, the responsivity of an InGaAs/InP *p-i-n* PD with similar absorbing layer thickness is around 0.5 A/W at a bias of ~1–2 V.[12] The electrical gain of the HPT component of the hybrid upconverter was therefore estimated to be 94. Figure 4b shows the measured luminance efficiency of the OLED part of the hybrid upconverter. The luminance efficiency first increased

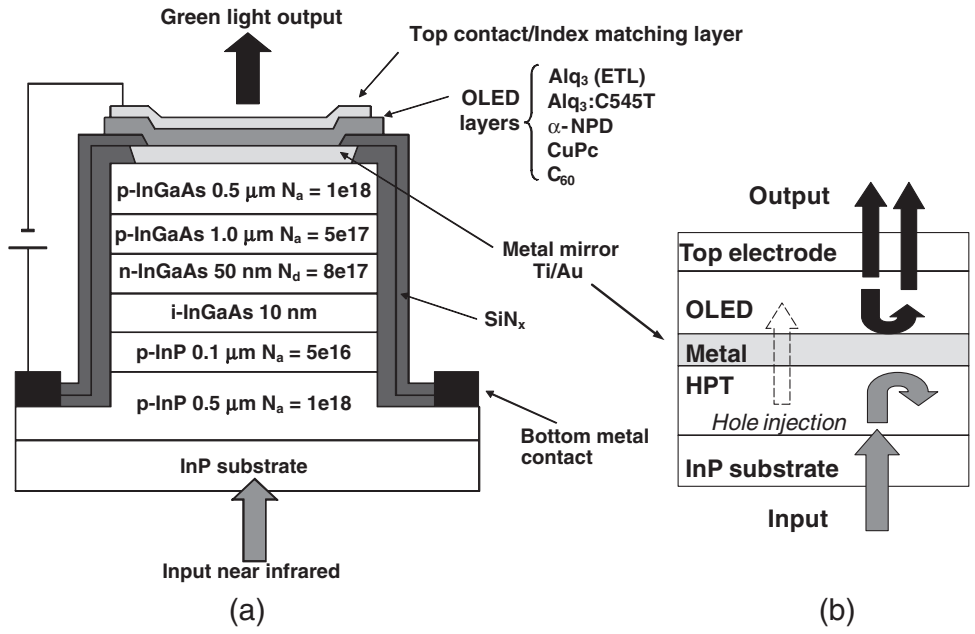


**Figure 2.** (a) Schematic cross section of hybrid optical upconverter device with integrated InGaAs/InP HPT and OLED. Note that the thickness of the organic and inorganic layers is not to scale. The embedded mirror layer consists of 20-nm Ti and 100-nm Au. The hole injection layer (HIL) of the OLED was a 3-nm thick layer of fullerene ($C_{60}$). The hole transport layers (HTLs) consisted of copper phthalocyanine (CuPc) (25 nm) and N,N′-diphenyl-N,N′-bis-(1-naphthyl)-1–1′-biphenyl-4,4′-diamine ($\alpha$-NPD) (45 nm). The 30 nm thick emission zone was tris-(8-hydroxyquinoline) aluminum ($Alq_3$), doped with 1 wt.% 10-(2-benzothiazoly)-1,1,7,7-tetramethyl-2,3,6,7-tetrahydro-1H, 5H, 11H-[1]benzo-pyrano [6,7,8-ij]quinolizin-11-one (C545T). The electron transport layer (ETL) was made of an additional 15 nm thick $Alq_3$ layer. The top metal contact consisted of LiF (1 nm)/Al (5 nm)/Ag (15 nm). Finally a 45-nm thick $Alq_3$ layer was refractive-index matching layer. No antireflection coating was applied to the back side of the InGaAs/InP sample. (b) The insertion of a highly reflective metal layer as an embedded optical mirror could improve the absorption and emission efficiency.

with the device bias. At ~10 V, it reached a maximum value of 7.6 cd/A, and then it decreased slowly with further increasing device bias. This phenomenon was also observed in Ref.[8] The luminance efficiency (cd/A) can be converted to OLED optical efficiency (mW/A) by assuming that the upconverter device is a Lambertian source and using 540 lm/W as the power conversion constant.[8] The calculated optical efficiency is also plotted in Figure 4b with a value of 33 mW/A under 21 V bias. The overall external power upconversion efficiency can then be calculated by multiplying the detector responsivity (A/W) and the OLED optical efficiency (mW/A), so the calculated value is 1.55 W/W at a bias of 21 V, which means the power of the output green light is 1.55 times of the input infrared light. The device exhibits optical upconversion with a power amplification. The NIR-to-visible photon conversion efficiency ($\eta_{con}$) can be calculated as follows,

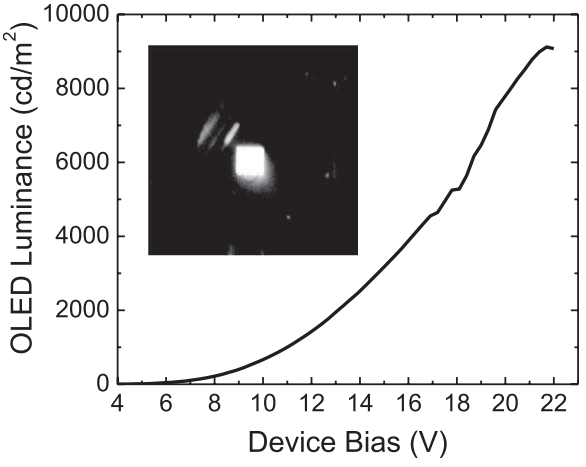


**Figure 3.** Luminance-voltage ($L$–$V$) curve of upconverter under 1.5-μm infrared illumination, with NIR power density of 1.2 mW/cm$^2$ [inset: image of hybrid upconverter operating at 15 V with input NIR from bottom].

$$\eta_{con} = \frac{\#\text{ of output photon}}{\#\text{ of input photon}} = \frac{\frac{P_{vis}}{h\overline{v_{vis}}}}{\frac{P_{NIR}}{hv_{NIR}}} = 1.55(W/W) \times \frac{hv_{NIR}}{h\overline{v_{vis}}} \quad (3)$$

where $P_{NIR}$ is the input light power, $P_{vis}$ the output visible-light optical power, $hv_{NIR}$ the NIR photon energy (= 0.83 eV), and $h\overline{v_{vis}}$ the averaged output visible photon energy, which is weighted by the relative emission spectrum intensity (see Supporting information,Figure S2).$h\overline{v_{vis}}$ is calculated to be 2.18 eV, and the NIR-to-visible photon conversion efficiency is 59%.

To demonstrate the NIR-to-visible light upconversion operation, the intensity of the output OLED emission was measured with different input NIR power densities. The results are plotted in **Figure 5**. Under dark condition (i.e., no input NIR illumination), the luminance of the green light emission from OLED was very low below a bias of 12 V. It increased above

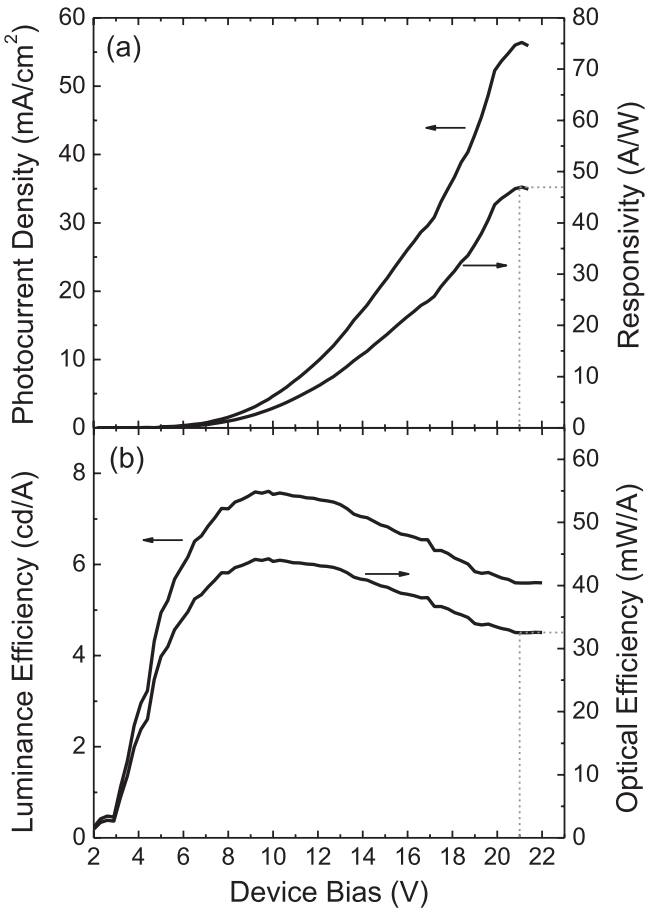


**Figure 4.** (a) Measured photocurrent density (mA/cm$^2$) as a function of device bias under 1.5-μm infrared radiation of 1.2 mW/cm$^2$ and the calculated responsivity (A/W) of the HPT component. (b) Measured luminance efficiency (cd/A) of the OLED component of the integrated upconverter and the calculated optical efficiency (mW/A). The power consumption of the integrated upconverter is 17.2 mW at 21 V bias with a total current of 0.82 mA.

12 V due to the amplified dark current by the HPT component. Possible origins of the dark current are structural defects from wafer growth and interface states formed at the integration of the HPT with the OLED, which needs to be clarified and suppressed for further improvement in device performance. With NIR illumination, the output luminance of the device became evident at a bias of ~9 V. As the NIR input power density increased from 0.12 to 1.2 mW/cm$^2$, the values of the output luminance at 21 V increased from ~4100 to ~9000 cd/m$^2$, clearly demonstrating the upconversion operation of the hybrid device at room temperature.

A NIR (1.5 μm) to visible light (green) electro-optical upconverter with amplified power gain has been designed and demonstrated. The device was fabricated by direct tandem integration of an OLED with an inorganic InGaAs/InP HPT. A built-in electrical gain of 94 from the HPT was achieved and an overall external power efficiency of 1.55 W/W (155% power efficiency) was measured at room temperature. This demonstration gives us strong confidence to exploit the utility of organic/inorganic hybrid semiconductor systems in making low-cost, large-area

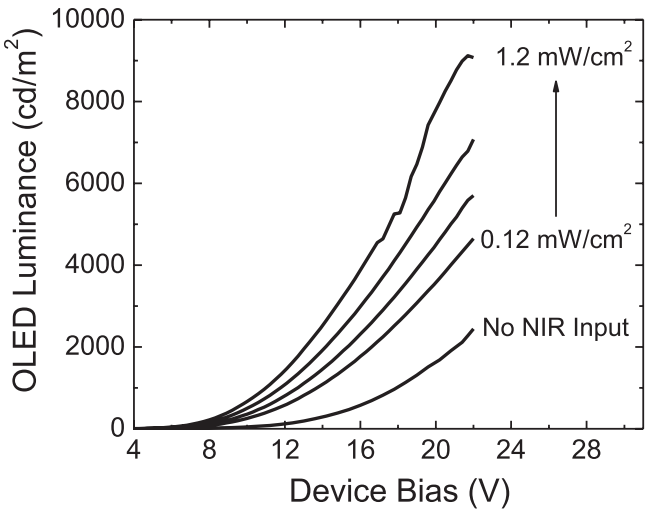


**Figure 5.** NIR-induced green light luminance as a function of device bias under different NIR illumination conditions (0.12 mW/cm$^2$, 0.3 mW/cm$^2$, 0.6 mW/cm$^2$, 1.2 mW/cm$^2$).

and high-efficiency NIR upconversion imaging devices. With the upconversion approach, imaging device can be realized with the tandem integration of an inorganic pixelated HPT array and a large-area single-element OLED. The continuous OLED layers on top of the HPT pixel array are expected not to cause significant lateral current spreading due to their poor lateral electrical conductivity and very thin thickness (~100–200 nm). The spatial resolution of the imaging device is mainly limited by the pixel size of the HPT part. The visible light emission from each individual pixel is triggered by the detection of input NIR radiation.

## *Experimental Section*

The optimized HPT was grown by chemical beam epitaxy (CBE) on a semi-insulating InP substrate. As shown in Figure 2a, the wafer growth started with an 500-nm InP emitter contact ($p^+$, $1 \times 10^{18}$ cm$^{-3}$) and a 100-nm InP emitter layer ($p$, $5 \times 10^{16}$ cm$^{-3}$). The growth continued with a 10-nm undoped InGaAs spacer and a 50-nm InGaAs base layer ($n$, $8 \times 10^{17}$ cm$^{-3}$). Then came a 1-μm InGaAs collector layer ($p$, $5 \times 10^{17}$ cm$^{-3}$). The structure was capped with a 500-nm InGaAs contact layer ($p^+$, $1 \times 10^{18}$ cm$^{-3}$). Si was used as the $n$-type dopant and Zn was used as the $p$-type dopant for the epilayers.

The first step of the device fabrication was to pattern and etch square mesas ($1 \times 1$ mm$^2$) onto the $p$-InP emitter. Square mesas were patterned using standard photolithography. A solution of $H_2SO_4$: $H_2O_2$: $H_2O$ (1:8:160) was used to etch the InGaAs layer (~1.6 μm thick) and another solution of $H_3PO_4$: HCl (10:1) was used to etch part of the $p$-InP layers (~0.2 μm thick) to complete the square mesas (Figure 2a). A 150-nm $Si_3N_4$ layer (SiN) was then grown on the top surface of the InGaAs/InP sample using plasma-enhanced chemical vapor deposition (PECVD). The SiN outside of the square mesa was etched off to form an open area, where a metal layer (Ti/Au) was deposited to serve as a common bottom contact. Square windows with a size of 0.9 mm × 0.9 mm were patterned using photolithography on top of the square mesas and chemically etched onto the SiN layer. The etching went through the entire SiN insulation layer to expose the semiconductor square mesa areas, on top of which an embedded metal mirror (Ti 20 nm/Au 100 nm) was deposited using electron-beam evaporation. A

second SiN layer was deposited to bury the metal mirror and was later partially etched off to expose a smaller window (0.8 mm × 0.8 mm) right on the top of the metal mirror. The second SiN layer was mainly for minimizing potential leakage current, which could significantly degrade device performance.

The InGaAs/InP substrate was then ultrasonically cleaned with a standard regiment of chloroform, acetone and methanol followed by ultraviolet (UV) ozone treatment for 30 minutes. Thereafter the sample was loaded into a Kurt J. Lesker LUMINOS cluster tool for deposition of the OLED. All molecular films were deposited sequentially through a shadow mask (15 mm × 15 mm opening) over the entire top surface of the substrate. Semi-transparent cathode metal electrodes (1.2 mm in diameter) were deposited on the top of the square mesa structures using a second shadow mask, without breaking vacuum. The top cathode layer was composed of LiF (1.0 nm)/Al (5.0 nm)/Ag (15 nm), which has an adequate sheet conductance, and is partially transparent to green light. Finally a 45 nm thick $Alq_3$ layer was deposited, which could provide better refractive-index matching from the LiF/Al/Ag to air.[14] Current-voltage-luminance (*I-V-L*) characteristics of the fabricated devices were measured with an HP 4140B picoammeter and a Minolta LS-110 luminance meter. The input 1.5 μm light was from a MPS-8033 precision fiber optic source. All measurements were conducted at room temperature, and under normal atmospheric condition.

## Supporting Information

Supporting Information is available from the Wiley Online Library or from the author.

## Acknowledgements

This work was supported by Natural Science and Engineering Research Council (NSERC) of Canada, Ontario Research Fund, University of Waterloo, National Research Council (NRC) of Canada and Dalsa Inc.. The first author would like to thank Saeed Fathololoumi and Kai Wang for useful discussions.

Received: May 26, 2010
Revised: July 8, 2010
Published online: August 23, 2010

[1] H. C. Liu, M. Gao, P. J. Poole, *Electron. Lett.* **2000**, *36*, 1300.
[2] J. S. Sandhu, A. P. Heberle, B. W. Alphenaar, J. R. A. Cleaver, *Appl. Phys. Lett.* **2000**, *76*, 1507.
[3] M. Chikamatsu, Y. Ichino, N. Takada, M. Yoshida, T. Kamata, K. Yase, *Appl. Phys. Lett.* **2002**, *81*, 769.
[4] M. J. Cohen, M. H. Ettenberg, M. J. Lange, G. H. Olsen, *Proc. SPIE* **1999**, *3698*, 453.
[5] D. Ban, H. Luo, H. C. Liu, Z. R. Wasilewski, M. Buchanan, *IEEE Photon. Technol. Lett.* **2005**, *17*, 1477.
[6] D. Y. Kim, D. W. Song, N. Chopra, P. D. Somer, F. So, *Adv. Mater.* **2010**, *22*, 2260.
[7] T. Rauch, M. Boberl, S. F. Tedde, J. Furst, M. V. Kovalenko, G. Hesser, U. Lemmer, W. Heiss, O. Hayden, *Nat. Photonics* **2009**, *3*, 332.
[8] D. Ban, S. Han, Z. H. Lu, T. Oogarah, A. J. SpringThorpe, H. C. Liu, *Appl. Phys. Lett.* **2007**, *90*, 093108.
[9] J. Chen, D. Ban, X. D. Feng, Z. H. Lu, S. Fathololoumi, A. J. SpringThorpe, H. C. Liu, *J. Appl. Phys.* **2008**, *103*, 103112.
[10] T. Moriizumi, K. Takahashi, *IEEE Trans. Electron. Dev.* **1972**, *19*, 152.
[11] M. Konagai, K. Katsukawa, K. Takahashi, *J. Appl. Phys.* **1977**, *48*, 4389.
[12] Y. C. Jo, S. J. Joe, H. Kim, P. Choi, *Jpn. J. Appl. Phys.* **2005**, *44*, 2537.
[13] L. Y. Leu, J. T. Gardner, S. R. Forrest, *J. Appl. Phys.* **1991**, *69*, 1052.
[14] L. S. Hung, C. W. Tang, M. G. Mason, P. Raychaudhuri, J. Madathil, *Appl. Phys. Lett.* **2001**, *78*, 544.